Curved folds in supported graphene under compression

Master Thesis

By

Aditya Vangal Vasudevan

CIMNE
Universitat Politecnica de Catalunya

A thesis submitted for the degree of
Master of Science in Computational Mechanics

Accomplished on
June 2013

Supervised by

Prof. Marino Arroyo
Department de Matematica Aplicada
and
Universitat Politecnica de Catalunya
Barcelona, Spain

Abstract

Atomically thin graphene is easily susceptible to out-of-plane deformation and tends to form wrinkles and folds. Wrinkles are small out-of-plane distributed buckling deformations, which coalesce under larger strains to form localized folds and these are commonly observed in single or few-layer graphene grown by Chemical Vapor Deposition (CVD). While in some applications, graphene is free-standing, most often it is adhered to a substrate (supported graphene) and has been shown to develop wrinkles and folds due to compressive strain. These deformations affect the electronic and chemical properties of graphene and hence it is important to control them. They depend on many factors and can be controlled by modifying the adhesion and friction between graphene and the substrate or by the anisotropy of strain. In this report, we try to control the position of folds by patterning the substrate into regions of high and low-adhesion. We focus on the possibility of curved folds in graphene and we find that under certain conditions curved folds that follow the prescribed pattern break into a collection of segmented folds. An explanation for the breaking pattern is given based on the strain energy, bending energy and adhesion energy. Application of curved folds could be in using the folds to focus graphene plasmonic waves for nanoelectronics or graphene based optical transistors. Another interesting application could be in nanofluidics to provide curved paths for nanofluidic flow.

Acknowledgement

I am extremely thankful to my advisor Prof. Marino Arroyo for giving me an opportunity to work on a very current topic and for his guidance throughout my thesis. I am also extremely thankful to my colleagues and friends in the lab, especially Kuan Zhang for helping me out with my research. I would also like to sincerely thank my parents for their continuous support and love all throughout my life. I gratefully acknowledge the Erasmus Mundus Category A grant awarded by the European Union for supporting my Master studies here in Barcelona.

Aditya Vangal Vasudevan
Barcelona, Spain.

Contents

List of Figures

Chapter 1

Introduction

Theoretically, graphene has been known to exist for over 60 years (Wallace, 1947; Slonczewski and Weiss, 1958) but only very recently in 2004 the material was discovered in free standing state (Novoselov et al., 2004) and since then the research on graphene has been phenomenal. Graphene is the name given to a flat monolayer of carbon atoms tightly packed into a two-dimensional (2D) honeycomb lattice, and is a basic building block for graphitic materials of all other dimensionalities(Geim and Novoselov, 2007). They can be wrapped into 0D fullerenes, 1D nanotubes and 3D graphite as shown in figure 1.1. Graphene has a planar structure and the carbon atoms in graphene are sp^2 hybridized. The C-C bond length in graphene is 0.142nm (Heyrovska, 2008).

The nobel prize for Physics was jointly awarded to Dr. Andre Geim and Dr. Konstantin Novoselov in 2010 for their discovery of graphene in 2004 and since then graphene has shown great promise as a future material for the electronic industry. In fact, it is often tagged as the material which will make possible the continuation of the Moore's Law(Moore, 1965). This is because of its physical, chemical and electronic properties which have been discussed in detail in the following section.

1.1 Properties of graphene

1.1.1 Electronic Properties

The interest in graphene is mainly due to its electronic and mechanical properties. The sp^2 hybridization between one s and two p orbitals leads to the formation of a trigonal planar structure with a formation of σ band between the s orbitals amd the formation of π band between the p orbitals perpen-

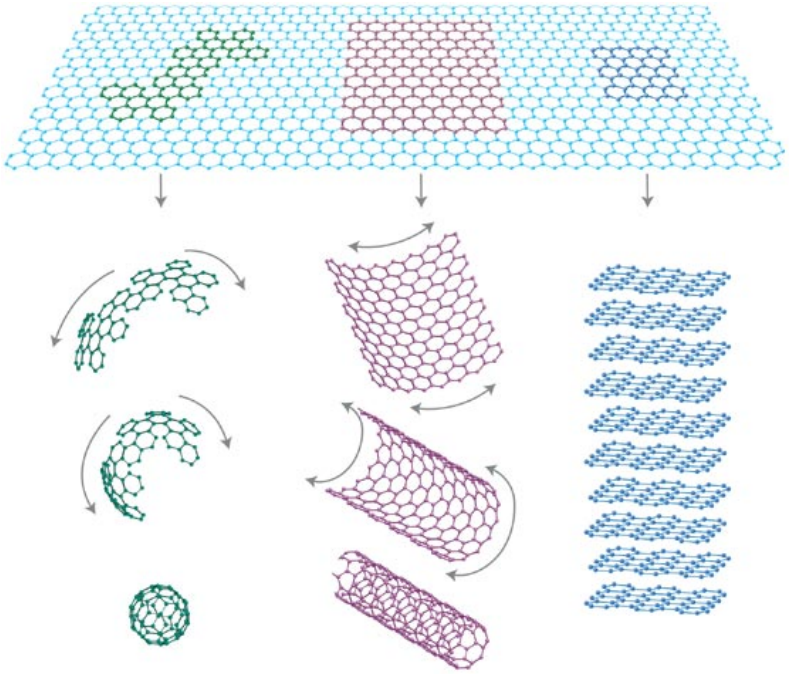

Figure 1.1: Atomic structure of graphene : It can be rolled into Nanotubes, stacked to form Graphite and wrapped to form Buckyballs [Taken from (Geim and Novoselov, 2007)]

dicular to the planar structure(Castro Neto et al., 2009). The π band is half filled and this gives graphene its interesting properties. One of the most interesting properties is that its low energy excitations are massless, chiral Dirac Fermions(Castro Neto et al., 2006a; Katsnelson M. I. and K., 2006; Katsnelson and Novoselov, 2007) . These Dirac fermions behave in unusual ways when subjected to a magnetic field and lead to intersting phenomena such as anomalous integer quantum Hall effect(Castro Neto et al., 2006; Novoselov K. S., 2005) at room temperature. It also is an intersting mix of a semiconductor (zero density of states) and a metal (gaplessness) giving it properties different from either. Also these properties can be modified by the application of an electric and magnetic field, chemical doping or addition of layers etc. which gives it a tremendous potential for applications ranging from chemical sensors to transistors(Geim and Novoselov, 2007).For a comprehensive review of the electronic properties please refer to (Castro Neto et al., 2009).

1.1.2 Mechanical Properties

Apart from the remarkable electronic properties, graphene has also very good physical properties. With an effective thickness of 0.335nm, the separation between layers of graphite, the Young's Modulus was reported around 1,100 GPa, a fracture strength of 125 GPa(Lee et al., 2008) which is 200 times the breaking strength of steel establishing it as one of the strongest materials ever measured. This motivates its use as Carbon-fibre reinforcements in advanced composites. But it was also found that the mechanical strength of graphene also depends on the defects present within the sheet and the type of edge terminations.

1.1.3 Thermal and other Properties

The thermal conductivity of single layer graphene is extremely high around $5{,}000\frac{W}{mK}$ and suggests that graphene can outperform nanotubes in heat conduction(Balandin et al., 2008). This high conductivity makes graphene a potential material for thermal management in electronic applications. The properties of graphene not only depends on itself, but also on the environment surrounding the graphene (Ishigami et al., 2007), for example the substrate, impurities in the substrate and the possibility of a water layer between graphene and the substrate(Sabio et al., 2008).

1.2 Synthesis of graphene

Graphene can be prepared using a variety of techniques and each technique have their advantages and disadvantages based on the quality of graphene produced and its properties depending on the substrate used. Some of the major preparation procedures of graphene are listed in this section.

1.2.1 Mechanical Exfoliation

Graphene was first prepared by the Manchester group led by Andre Geim in 2004 by the process of Mechanical Exfoliation(Novoselov et al., 2004). Also called as the scotch-tape process, the graphene prepared by them was made by repeated peeling of small mesas of highly oriented pyrolytic graphite(HOPG) by using adhesive tape. Using this approach they were able to prepare Few Layer graphene (FLG) films of upto 10 μm in size.

Fig 1.2 shows graphene prepared by the method of mechanical exfoliation. This graphene prepared were of remarkably high quality and they exhibited a room-temperature mobilities of $\tilde{1}0{,}000$ square centimeters per volt-second

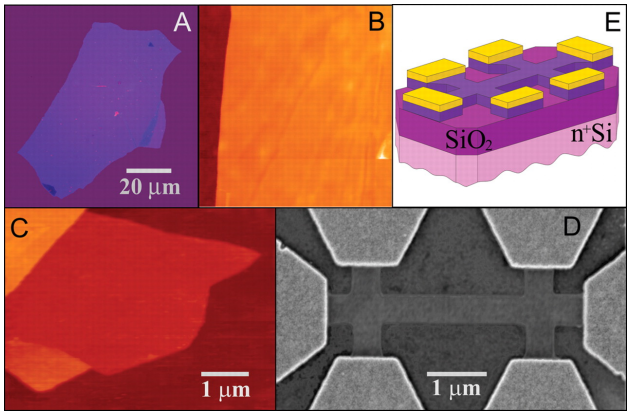

Figure 1.2: (A) Photo of large multilayer graphene flake in an oxidized Si Wafer, (B) Area of 2μ m by 2μ m of this flake near the edge (Dark Brown - Si Wafer, Orange - 3nm height above the SiO_2 surface, (C) AFM image of single layer graphene, (D) Scanning electron microscope image of the experimental device prepared from FLG, (E) Schematic view of the Device [Taken from (Novoselov et al., 2004)]

on the application of a gate voltage. High quality graphene was produced by this method, but this method is not scalable meaning one cannot make large areas of graphene which are actually required for the fabrication of electric devices.

1.2.2 Epitaxial growth on Silicon Carbide

Graphene can be made by another method by thermal decomposition of Silicon Carbide (SiC) to a temperature of 1100 degrees Celsius at low pressures which reduces it to graphene.

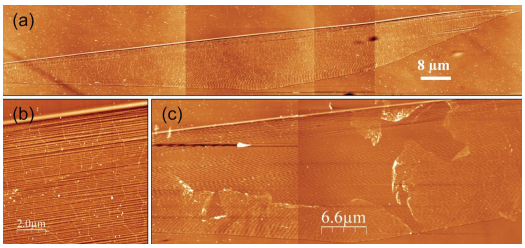

Figure 1.3: AFM image of epitaxial graphene grown on a 4H-SiC substrate (a) at a large scale, (b) showing the wrinkle and step bunched character of SiC below, (c) a layer scratched by AFM tip [Taken from Camara et. al. (Godignon and Camassel, 2011)]

Fig. 1.3 shows the Atomic Force Microscopy (AFM) images of Epitaxial Graphene (EG) grown from SiC. The ultrathin epitaxial graphene shows remarkable 2D electron gas behaviour (2DEG) and the material can be easily patterned using nanolithography (Berger et al., 2004, 2006).

1.2.3 Chemical Vapor Deposition of graphene on Metal Substrates

This is another popular way of preparing graphene by depositing it on metal substrates like Cu, Ni, Pd and Ir. The growth of graphene on Ni gives monolayer and few layer graphene. The multilayer graphene is formed due to the presence of grain boundaries on Ni films (Zhang et al., 2013). The multilayers in graphene can be avoided when grown on Ni substrates if the substrate is Ni(111) cause these have smooth surfaces and do not have grain boundaries. Another important metal in the preparation of graphene by CVD is copper, Cu. As the solubility of carbon is very low in Cu, this substrate is even better than Ni and has resulted in larger amounts of single layer graphene.

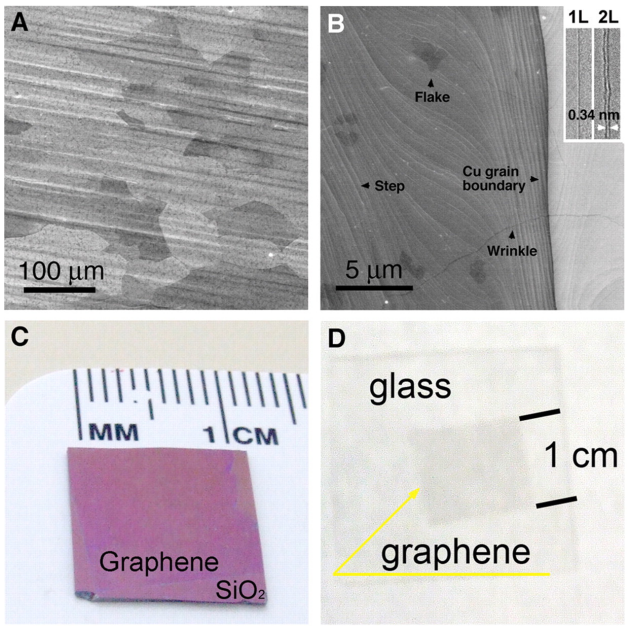

Figure 1.4: (*A*) SEM image of graphene grown by CVD on copper, (*B*) SEM image showing graphene wrinkles, Cu grain boundary and steps and two-and three- layer graphene flakes, (*C and D*) graphene transfered from Cu to SiO_2 and Glass substrates respectively [Taken from Li et. al. (Li et al., 2009)]

Fig 1.4 shows a picture of graphene grown on Cu substrate by Chemical vapor deposition. An important feature of graphene obtained by CVD is that the graphene obtained is polycrystalline in nature with the formation of grain boundaries (Kim et al., 2009). Typically, for graphene to be used in nanoelectronic and photvoltaic applications, it has to be transfered from the metal substrate to a substrate like SiO_2 or Si wafer. This can be done easily by the process of etching. For a more comprehensive review of graphene obtained by CVD please refer to (Zhang et al., 2013) and (Mattevi et al., 2011)

1.3 Wrinkling on graphene : Motivation

As mentioned in section 1.2.3 CVD is one of the popular techniques to make larger area of graphene, but this method has some disadvantages as well. As graphene is a very thin material, it is easily susceptible to out-of-plane deformations and this leads to the formation of wrinkles and folding patterns on a layer of graphene. For length scales $l > 100h(\sim 10nm)$, much greater than the mechanical thickness of graphene, it was found to be prone to out-of-plane buckling deformations to relax the in-plane deformations or conform to an elastic wavy substrate(Li and Zhang, 2010; Scharfenberg et al., 2012). These deformations or corrugations in the third dimension can be seen as a stability mechanism for thin two-Dimensional films (Meyer et al., 2007).

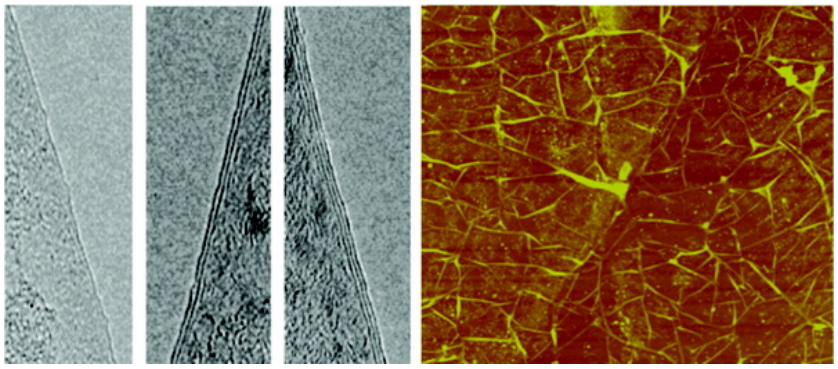

Figure 1.5: (left)TEM image showing one,two and three layer graphene obtained by CVD respectively (Right) AFM image showing the wrinkling of graphene on SiO_2 using PMMA as support polymer [Taken from Srivastava et. al. (Srivastava et al., 2010)]

Fig 1.5 shows the AFM image of wrinkling on SiO_2 using PMMA as support polymer (Here, graphene was first deposited on Copper using CVD

technique and was then chemically etched to SiO_2 with a PMMA support by chemical etching (Srivastava et al., 2010). In the manufacture of graphene by CVD on a large area, the graphene and the copper film are both heated to very high temperatures. The thermal expansion coefficient for graphene is $\alpha_{graphene} = -6 \times 10^{-6}/K$ (Chris and Ning, 2009) while that for copper is $\alpha_{Cu} = 24 \times 10^{-6}/K$ (Nelson and Riley, 1945). Thus the wrinkles in the graphene can be attributed to the difference in the thermal expansion coefficients between graphene and copper. Upon cooling, there is a significant compressive strain on graphene and this causes the wrinkling pattern on graphene.

The wrinkles present in graphene in turn affect the electronic properties of graphene under the presence of an electric or magnetic field. Scanning tunneling spectroscopy measurements identify the existence of electron pockets at the higher levels of ripples (Vázquez de Parga et al., 2008) and the wrinkling creates a spatially varying electrochemical potential proportional to the square root of the curvature (Kim and Neto, 2008). A more comprehensive review on the electronic properties due to ripples can be found in (Guinea et al., 2008a,b; Katsnelson and Geim, 2008). Hence it is necessary that we be able to control the wrinking pattern in a graphene layer so that it can be exploited productively to design devices based on local strain and selective bandgap engineering(Elias et al., 2009). Based on the strain engineering concept, we can use strain for making 1D channels, surface states and confinement on graphene , all of which are required for the design of devices(Pereira and Castro Neto, 2009). Another way to control the wrinkles is by chemically patterning the substrate to high and low adhesion zones(Vandeparre et al., 2007). Surface wrinkles can also in turn be used to create zones of high and low adhesion as has been applied to the development of smart adhesives (Chan EP and AJ, 2008). Thus it is necessary to understand the mechanism of wrinkling and folding in graphene so that it can be understood and exploited to our gain.

In the work of Kuan Zhang (Zhang and Arroyo, 2013) in the same research group, the influence of adhesion and friction on the wrinkling and folding of graphene was studied. It was observed that under a small compressive strain distributed wrinkles are formed which transit to a fold.

Figure 1.6 shows the wrinkle-to-fold transition of graphene under uniaxial compressive strain. The energy of the system can be seen as a sum of three energies viz. the in-plane stretching energy, the bending energy and the non-bonded interaction energy. The in-plane stretching energy is due to the in-plane stretching of the membrane and for the simulation in Fig. 1.6 there is very less stretching and hence its contribution is very small. The bending energy is due to the out-of-plane deformation and the non-bonded

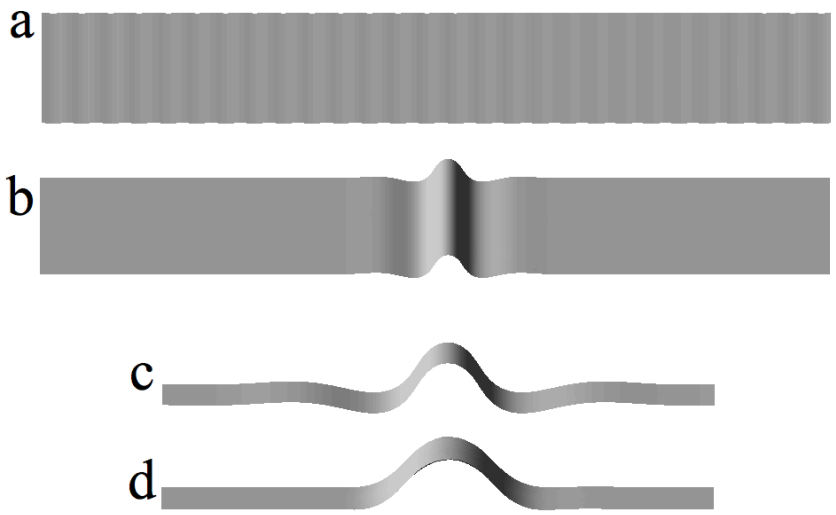

Figure 1.6: The wrinkle-to-fold transition of a graphene layer of length 200 nm, with $\gamma = 0.45J/m^2$. (a) the onset of wrinkling for $h_0 = 6nm$, (b) wrinkles transit to a fold for $h_0 = 6nm$, (c) Cross-section of the fold for $h_0 = 6nm$, (d) Cross-section of fold for $h_0 = 0.6nm$ [Taken from (Zhang and Arroyo, 2013)]

interaction energy is the interaction energy between the atoms of graphene and the substrate. Under compressive strain, graphene tries to bend out-of-plane, but the adhesion energy penalizes this deformation and the wrinkle and fold formation can be seen as a competition between the bending and the adhesion energy. If the substrate is placed at a distance out of the influence of the adhesion energy (low equilibrium distance, h_0, refer section 2.2.2), then the influence of adhesion energy is lower and no wrinkles are observed in these cases (as seen in (d) of figure 1.6) and a fold is formed directly. The position of a straight fold can be controlled by patterning the substrate into regions of different adhesion. Figure 1.7 shows the formation of fold formed in graphene due to uniaxial strain. The adhesion energy in the substrate is reduced in the stripe beneath the fold so that the graphene is allowed to have larger out-of-plane deformations in this zone and thus directing the fold to be formed at this point.

The main goal of the work was to test the possibility of curved folds on graphene by patterning the substrate into curved regions of low adhesion and to test how the folding pattern varies with the application of strain and different curvatures of curved folds.

The outline of the report is as follows. Chapter 2 explains the simulation methodology viz. the atomistic-based continuum model and the energy cal-

Figure 1.7: Position of fold controlled by patterning the substrate. The adhesion energy is removed in the strip beneath the fold so that the fold can be directed here

culations for studying the folding pattern in graphene. Chapter 3 shows the simulations and results for curved folding patterns on graphene and Chapter 4 gives the conclusion from the obtained results.

Chapter 2

Simulation Methodology

As graphene is a layer one atom thick, an atomistic-based continuum model by (Arroyo and Belytschko, 2002) is used. The kinematic setting follows the notations in the papers by Arroyo and Belytschko and a brief description of the model is given in this chapter. For a detailed review on the model, the reader is referred to these papers (Arroyo and Belytschko, 2002, 2004). Numerical simulations are performed by finite elements using the method of Subdivision Surfaces (Cirak et al., 2000) based on classical Loop scheme.

2.1 Exponential Cauchy Born rule

The Born rule is one of the standard methods used to link the deformation of an atomistic system to a continuum model. In this section, a brief introduction is given to the standard Born rule and then its limitiations and the necessity of an exponential map is given.

2.1.1 Standard Born Rule

Also referred by *Method of Homogeneous Deformations*, it says, the crystal vectors defined by two nuclei deform according to the local deformation gradient. Mathematically this can be written as

$$a = FA \tag{2.1}$$

where a is the deformed crystal lattice vector and A is the undeformed crystal lattice vector and F is the deformation gradient.

Once the deformed crystal lattice vectors are calculated, the length and the angle made by the vectors can be calculated by using simple continuum mechanics relations. For the case of bulk materials, the standard Born rule

works very well but it fails to extend to the case of crystalline flims and one-atom thick membranes. In the standard born rule, the lattice vectors are connected by the deformation gradient which maps the tangent spaces whereas the deformation of the bonds depends on the behaviour of the chords to the surface. This can be easily understood by a simple example considering the undeformed shape as planar and then it is rolled to deform to a cylinder but without stretch. Using the standard Born rule, for the same point the deformed and the undeformed lattice vectors are coplanar lying on the tangent plane to that point. Thus, there is no change in the geometric quantities and there is no change in the energy of the system upon rolling. However the deformed and undeformed vectors do not remain coplanar and their lengths change. Thus, for the simulation of zero-thickness membranes, the exponential born rule is used.

2.1.2 Exponential Map

According to standard definition, (Morgan, 1993) the definition of the exponential map for a manifold M is given by :

" The exponential map $\exp_p$ at a point p in M maps the tangent space T_pM into M by sending a vector $\mathbf{v}$ in T_pM to the point in M a distance $|\mathbf{v}|$ along the geodesic from p in the direction $\mathbf{v}$"

The exponential map is both differentiable and invertible in the neighborhood of the point p and hence the inverse exponential map can be used to send a vector from the crystal lattice to the vector space too. The exponential map is used to extend the Born rule for the case of atomically thin films as well.

Let Ω_0 and Ω represent the undeformed and the deformed body while $\mathbf{A}$ and $\mathbf{a}$ represent the crystal lattice vectors in the respective configuration. Let us assume that the vector $\mathbf{A}$ joins the two points $\mathbf{X}$ and $\mathbf{Y}$ on the undeformed body and that $\mathbf{Y}$ is sufficiently close to $\mathbf{X}$ so that the inverse of the exponential map can be applied. Using the inverse exponential map, we can define a vector $\mathbf{W}$ in the tangent space of Ω_0 at $\mathbf{X}$, $\mathbf{T_X}\Omega_\mathbf{0}$. Using the deformation gradient, $\mathbf{F}$ this vector $\mathbf{W}$ can be transformed to a vector $\mathbf{w}$ in the tangent space of $\mathbf{x}$, $\mathbf{T_x}\Omega$ and using the exponential map, $\mathbf{w}$ can be sent to a point $\mathbf{z}$ making the lattice vector $\mathbf{a}$ a chord to the surface Ω between $\mathbf{x} = \Phi(\mathbf{X})$ and $\mathbf{z}$.

Mathematically the exponential Born rule can be written as

$$\mathbf{a} = \mathfrak{F}_\Phi(\mathbf{A}) := exp_{\Phi(\mathbf{X})} \circ \mathbf{F}(\mathbf{X}) \circ exp^{-1}_{\mathbf{X}}(\mathbf{A}) \tag{2.2}$$

As the undeformed shape for Graphene is planar, this equation simplifies to

$$\mathbf{a} = \mathfrak{F}_{\Phi}(\mathbf{A}) := exp_{\Phi(\mathbf{X})} \circ \mathbf{F}(\mathbf{X})\mathbf{A} \tag{2.3}$$

Thus, given the undeformed lattice vector, we can obtain the deformed lattice vector based on the deformed surface. The deformed lattice vectors in general can be written as

$$a_i = f(\mathbf{C}, \mathcal{K}; \mathbf{A_i}) \tag{2.4}$$

and

$$\theta_{jk} = g(\mathbf{C}, \mathcal{K}; \mathbf{A_j}, \mathbf{A_k}) \tag{2.5}$$

where a_i and A_i are the length of the deformed and undeformed lattice vector respectively, $\mathbf{C}$ is the Green deformation tensor, $\mathcal{K}$ is the curvature tensor, and θ_{jk} is the angle between lattice vectors a_j and a_k

2.2 Elastic Potential

This section presents the construction of the hyper-elastic potential for the graphene layer. The energy is basically due to two kinds of interactions viz. the covalent bonded interaction and the long range or non-bonded interaction. An atomistic model is used to calculate the interactions and with the help of the exponential born rule which links the atomistic to a continuum model, the hyper-elastic potential is formulated. These interactions and their formulations are exlained in detail in the following sections.

2.2.1 Bonded Interactions

These interactions are due to the covalent bond between the Carbon atoms. It is assumed in this model that there is no bond-breaking or rearranging during deformation. The bonded interaction energy can be given in terms of the bond geometry i.e. the length and the angle between the adjoining bonds.

$$E = E(r_i, \theta_j) \tag{2.6}$$

Several atomistic models exist for the calculation of the bonded interaction. In our simulation the Brenner potential for hydrocarbons is considered(Brenner, 1990), which calculates in the interaction in terms of bond order potentials. According to this model, the bonded energy is written as a sum over atomic site i

$$E_b = \frac{1}{2}\sum_i E_i \tag{2.7}$$

where each E_i is given as

$$E_i = \sum_{j(\neq i)} [V_R(r_{ij}) - B_{ij}V_A(r_{ij})] \tag{2.8}$$

In equation 2.8 the sum is over nearest neighbors j of atom i, $V_R(r)$ and $V_A(r)$ are repulsive and attractive interactions respectively and B_{ij} is the normalized bond order potential. In our simulations we have used the Brenner potential, but for completeness the 2-body/3-body expansion is also listed and according to this model, the potential is given by

$$E = \sum_i V_s(r_i) + \sum_k V_\theta(\theta_k, r_k^1, r_k^2) \tag{2.9}$$

where the first sum is over the covalent bonds and the second sum is over the angles formed by the bonds. r_k^1 and r_k^2 denote the lengths of the chords forming the angle θ_k. Plugging equations 2.4 and 2.5 into the energy potentials, we can write the strain energy density as

$$W = W(\mathbf{C}, \mathcal{K}, \eta_\mathbf{k}) = \frac{1}{S_0} E_{cell}(\mathbf{a}(\eta_\mathbf{k}), \theta_\mathbf{jk}) \tag{2.10}$$

where $\eta_\mathbf{k}$ are the inner displacements due to the shifts of simple Bravais lattices. The strain energy is then minimized with respect to the inner displacements and after this inner relaxation, the energy density can be written only in terms of the local deformation as

$$W = W(\mathbf{C}, \mathcal{K}, \hat{\eta_\mathbf{k}}(\mathbf{C}, \mathcal{K})) = \hat{W}(\mathbf{C}, \mathcal{K}) \tag{2.11}$$

The internal energy of the membrane is then given by

$$W = \int_{\Omega_0} W(\mathbf{C}, \mathcal{K}) d\Omega_0 \tag{2.12}$$

2.2.2 Non-Bonded or Van der Waals Interactions

This interaction is calculated only for the pairs which are not directly bonded with each other but are still within close vicinity to each other. To calculate the Van der Waals interaction, we have used the Lennard-Jones potential. The Lennard-Jones potential gives the energy of two non-bonded atoms or

molecules based on their distance of separation. It is given by the 12-6 Lennard-Jones potential (Girifalco et al., 2000)

$$V(r) = 4\epsilon \left[\left(\frac{\sigma}{r}\right)^{12} - \left(\frac{\sigma}{r}\right)^{6} \right] \tag{2.13}$$

or

$$V(r) = \epsilon \left[\left(\frac{r_m}{r}\right)^{12} - 2\left(\frac{r_m}{r}\right)^{6} \right] \tag{2.14}$$

where ϵ is the depth of the potential well, σ is the distance at which the potential is zero and r_m is the equilibrium distance, the distance where the potential reaches the minimum and r is the distance between the atoms or molecules. At r_m the potential is $-\epsilon$. The equilibrium distance, r_m, is the distance between the molecules for which the potential is minimum. The equilibrium distance and σ are related by the equation

$$r_m = 2^{1/6}\sigma \tag{2.15}$$

Figure 2.1 shows the 12-6 Lennard Jones potential with relative axes r/σ and V/ϵ. From the graph we can see that when the molecules are very far apart, the potential is zero thus implying no non-bonded interaction. As the molecules come closer, there is an attraction force and the potential energy becomes negative and is minimum at the equilibrium distance. Beyond the equilibrium distance, repulsive forces dominate and the potential becomes positive again. For carbon-carbon interactions, we take the values as ϵ= 0.00153 aJ and $r_m = 0.3834$ nm.

We are interested in deriving the energy-density per unit area for the interactions between graphene and the substrate. The effective point-half space interaction energy is of the form (Aitken and Huang, 2010)

$$V = -\gamma \left[\frac{3}{2}\left(\frac{h_0}{h}\right)^{3} - \frac{1}{2}\left(\frac{h_0}{h}\right)^{9} \right] \tag{2.16}$$

where h is the separation between graphene and the planar substrate, h_0 is the equilibrium distance and γ is the adhesion energy between graphene and the substrate. For graphene and SiO_2 the adhesion energy is $0.45 J/m^2$. Figure 2.2 shows the effective point-half space interaction energy and the equilibrium distance h_0 and γ We integrate the non-bonded potential along the surface area of Graphene to get the non-bonded energy as

$$W = \int_{\Omega_0} V dS_0 \tag{2.17}$$

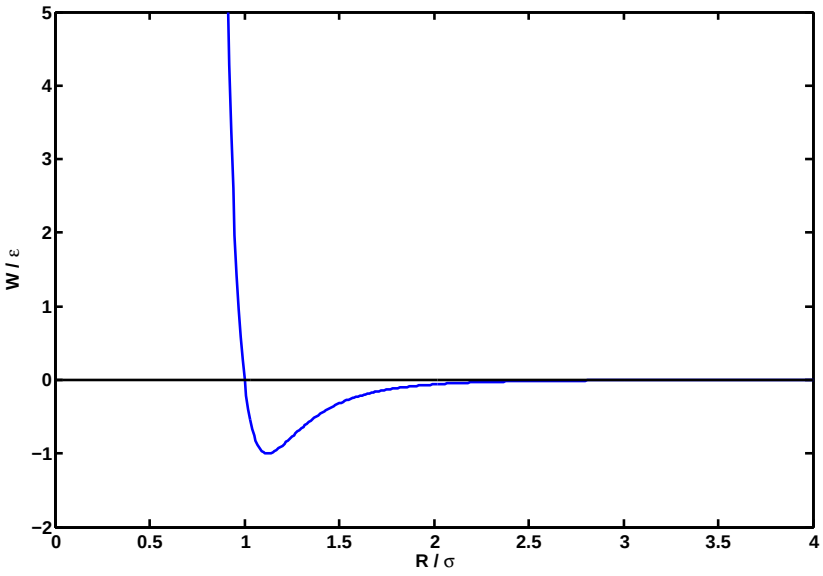

Figure 2.1: 12-6 Lennard Jones potential. The graph is with relative axes r/σ and V/ϵ

2.2.3 Body force

Let $\mathbf{B}$ be the external force (like electrostatic) per unit undeformed area. Then the corresponding potential is

$$W = \int_{\Omega_0} \mathbf{B} \cdot \Phi d\Omega_0 \tag{2.18}$$

Thus adding equations 2.12, 2.17 and 2.18 we calculate the total potential energy of a given deformation map Φ

$$\Pi(\Phi) = \Pi_{int} + \Pi_{nb} - \Pi_{ext} \tag{2.19}$$

that is,

$$\Pi(\Phi) = \int_{\Omega_0} W(\mathbf{C}, \mathcal{K}) d\Omega_0 + \int_{\Omega_0} V dS_0 - \int_{\Omega_0} \mathbf{B} \cdot \Phi d\Omega_0 \tag{2.20}$$

This potential energy is minimized to calculate the stresses.

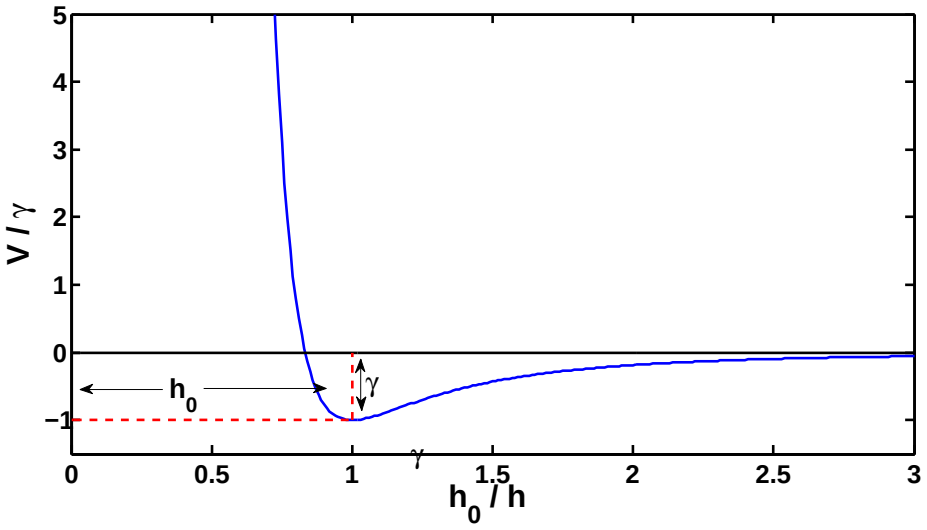

Figure 2.2: The effective point-half space interaction energy

2.3 Numerical Implementation

The minimization of the potential energy leads to derivatives of the curvature tensor and hence for the numerical implementation, we need the shape functions to be atleast H^2. Hence for the finite elements, the method of subdivision surfaces (Cirak et al., 2000) based on the Loop scheme is used. The interpolation scheme implemented in this method is non-local, i.e. the shape functions not only depend on the nodes in one element but also on the nodes on the immediate neighboring elements as well which gives nice square integrable functions whose first- and second-order derivatives are square integrable. The stable configuration is obtained by minimizing the energy in equation 2.20 using a quasi-Newton method, the L-BFGS algorithm as implemented by Liu and Nocedal (Arroyo and Belytschko, 2002). The simulations are done using periodic boundary conditions and compressive strain is applied to this periodic box.

The next chapter reports the results for the simulation of Graphene on SiO_2 substrate. Curved patterns where formed on the substrate by pattern-

ing into regions of high and low adhesion energy.

Chapter 3

Simulation of Curved Folds

In this chapter we report our study on the curved folds on a single layer of graphene on an SiO_2 substrate. As mentioned before, the main idea is to see if it is possible to obtain curved folds on graphene. To perform the simulations a parallel code written in FORTRAN was used and executed on 32 nodes in the cluster owned by *Laboratori de Càlcul Numèric*, resulting in a computation time of approximately 1 day per simulation.

3.1 A typical fold

Fig. 3.1 below shows the top and the cross-section view of a typical curved fold. This simulation has been done for a graphene layer of 500 by 500 nm dimension, an equilibrium distance of $h_0 = 0.6$ nm, an amplitude of 35 nm for the pattern and an adhesion energy $\gamma = 0.45 J/m^2$ (refer section 2.2.2 and equation 2.16). Compression is applied to the graphene layer uniaxially and only in the X-direction reducing the length by 0.05 % at every step. The rate has been set very slow so as to obtain the most stable configuration. The simulation has been done with approximately a total of $\sim 10^6$ nodes and $\sim 10^7$ atoms.

The Van der Waals energy is an interaction energy between the atoms of the substrate and the Graphene layer (refer section 2.2.2). To control the region of the fold, the Van der Waals interaction is removed at that region, so that the separation occurs in that region (creating a region of low adhesion). This interaction energy is removed by multiplying the original energy with a Gaussian distribution. A Gaussian distribution is chosen because it gives a continuous transition of the energy to zero. Physically, this can be thought as a pattern on the substrate without material or weak adhesion. Several experiments have been carried out to control the wrinkling on thin films by

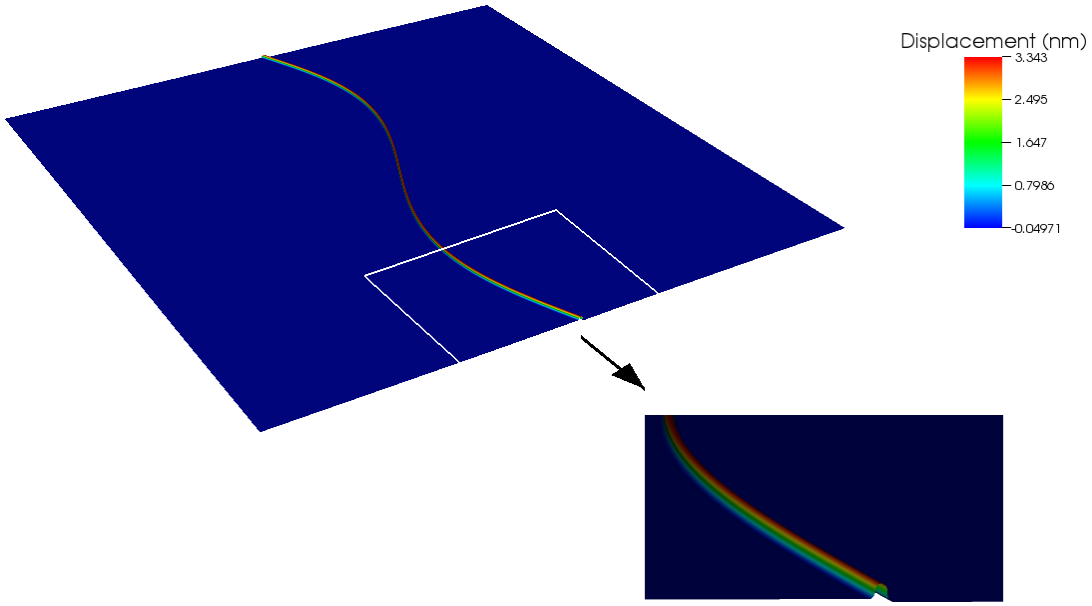

Figure 3.1: Top and cross-section view of a typical fold,
L = 500 nm, $\gamma = 0.45\text{J/m}^2$, $h_0 = 0.6nm$, A = 35 nm

patterning the substrate into regions of high and low adhesion (Vandeparre et al., 2007). A typical Gaussian distribution is of the form

$$f(y) = a \exp\Big[-\frac{(y-b)^2}{2c^2}\Big] \tag{3.1}$$

We multiply the Van der Waals energy with $1 - f(y)$ so that the Van der Waals interaction is removed only at the region where the fold is desired. The size and the position of the fold is controlled by the three parameters a, b and c. a is a dimensionless quantity and gives the amplitude of the Gaussian distribution and it is chosen as unity. c gives a measure of the width of the fold. Based on previous simulations a typical width of fold was 4nm. For a value of $c = 1\ nm$ the width of the gaussian distribution at one-tenth of a maximum is given by $2(\sqrt{2ln10})c$ which is around 4nm. Hence a value of c=*1 nm* is chosen for our simulations. To obtain a curved fold, the value of b is chosen to be a sinusoidal function of x so that the fold follows a sinusoidal curve. Before trying a curved sinusoidal curve, many other curves such as cosine and arctan were also considered but the results of the sinusoidal curve are only reported. As we are performing the simulation with periodic boundary conditions, the sinusoidal fold must also satisfy periodic boundary conditions. The value of b is given as

$$b = A \sin\Big[\frac{\pi}{250}(x + 250)\Big] \tag{3.2}$$

where A is the amplitude of the pattern. We thus multiply the Van der Waals interaction energy with *1 - f(y)* to obtain a sinusoidal fold on Graphene.

3.2 Breaking pattern of the folds

A uniaxial strain is applied to the graphene and as we increase the strain, we observe that the fold breaks from a curved shape to straighter segments. Fig. 3.2 shows the breaking pattern of the fold for an aplitude of 35 nm with increasing strain.

We can see from Fig. 3.2 and Fig 3.3 that the fragmentation into segments is possible in two ways namely by the increase in the strain or by the increase in the amplitude of the pattern. As we increase the amplitude of the pattern, we can observe from 3.3 that the fold breaks into more number of segments and they have a lower fragmentation strain too. In Fig. 3.2 it can be noted that distributed wrinkles do not seem to form prior to folding. This is because these simulations have been performed at low equlibirium distances and for these values we do not have any wrinkling zone (refer Section 1.3)

3.3 Explanation for breaking pattern based on Energies

There are basically three main energies involved in this simulation. They are the in-plane strain energy, bending Energy and Van der Waals Energy. These are discussed one-by-one in detail as follows.

3.3.1 In-plane Strain Energy

The in-plane strain energy is the energy due to the stretching of the graphene layer at the fold. Fig. 3.4 shows the variation of the total strain energy with the increase in strain for different amplitudes of the sinusoidal pattern. The strain is applied in steps and for each step the dimension of the periodic box is reduced by 0.05 %. For the first 16 steps ($\epsilon = 0.797\%$, the highest peak), the strain energy gradually increases from zero to a maximim value. As these simulations have been performed for graphene with a small equlibirium distance, we do not see any wrinkles and a fold is formed directly

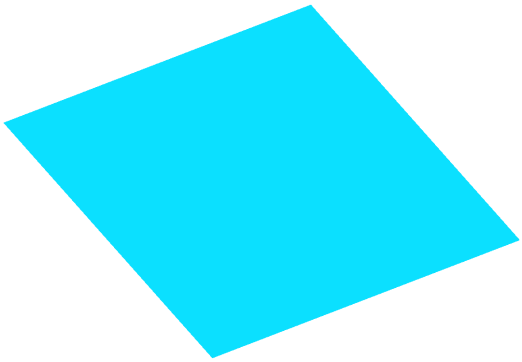

(a) $\epsilon = 0.75\%$

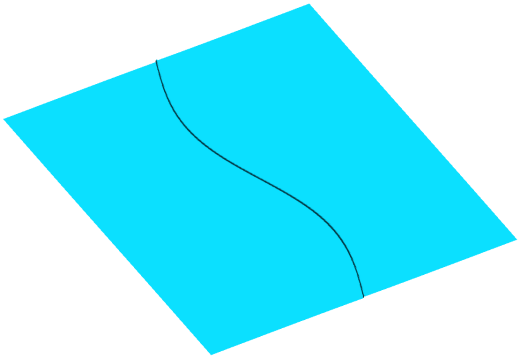

(b) $\epsilon = 1.2\%$

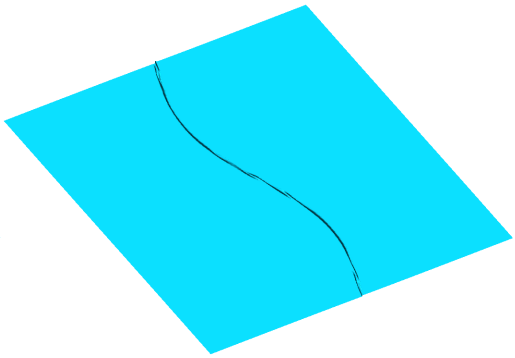

(c) $\epsilon = 1.63\%$

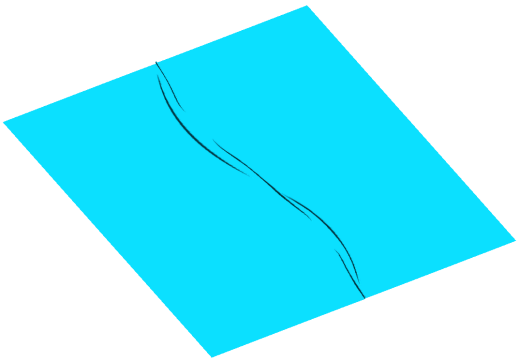

(d) $\epsilon = 1.74\%$

Figure 3.2: Breaking pattern of curved fold with increasing strain, $A = 35$ nm

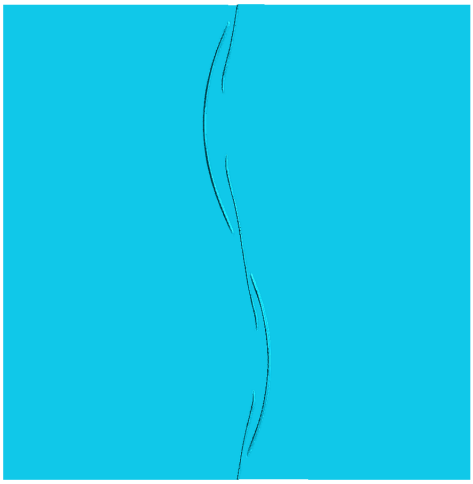

(a) $\epsilon = 1.63\%, A = 35nm$

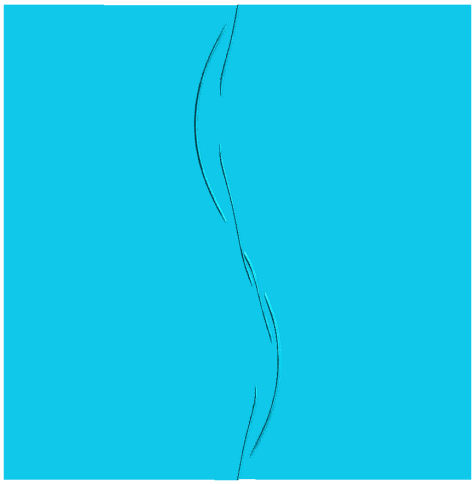

(b) $\epsilon = 1.48\%, A = 45nm$

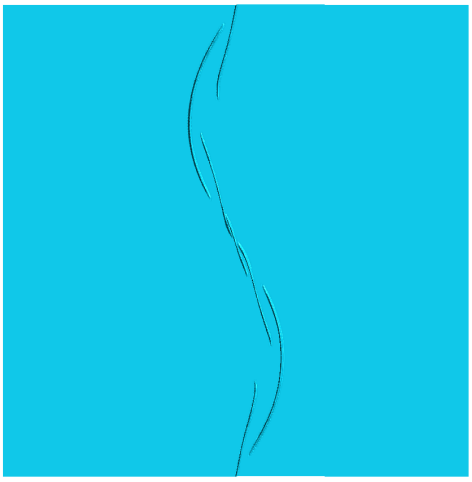

(c) $\epsilon = 1.43\%, A = 50nm$

Figure 3.3: Change in pattern with increase in Amplitude

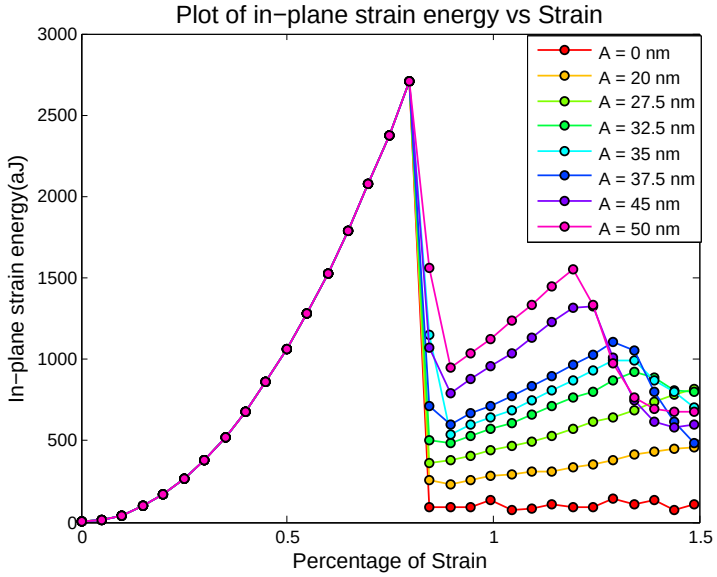

Figure 3.4: Variation of total Strain Energy for different Amplitudes

(refer section 1.3). This fold releases the in-plane strain energy and it falls down to a lower value. As the strain is continued to increase, we observe that the strain energy again increases. This increase in strain energy can be attributed to the increase in the Gaussian Curvature of the fold.

The Gaussian Curvature of a point on a surface is the product of the two princpal curvatures κ_1 and κ_2. Thus the Gaussian Curvature K can be written as

$$K = \kappa_1 \kappa_2 \tag{3.3}$$

The principal curvatures are the maximum and the minimum curvatures of the curves formed by different planes containing the normal at that point. For example, for a cylinder, the principal curvatures are $\frac{1}{R}$ and 0, where R is the radius of the cylinder. Hence the Gaussian curvature for the cylinder is the constant zero. According to Gauss Egregium theorem, a deformation of a planar sheet without stretching has zero gaussian curvature. A non-zero Gaussian curvature implies that there is stretching in the surface and that surface cannot be made from a plane sheet of paper without crumpling. For example, see (Dias and Santangelo, 2012). For example a sphere, whose curvature is $\frac{1}{R^2}$ cannot be made from a plane sheet of paper without crumpling while a cylinder can be.

In our case of curved folds on Graphene we can observe that there is

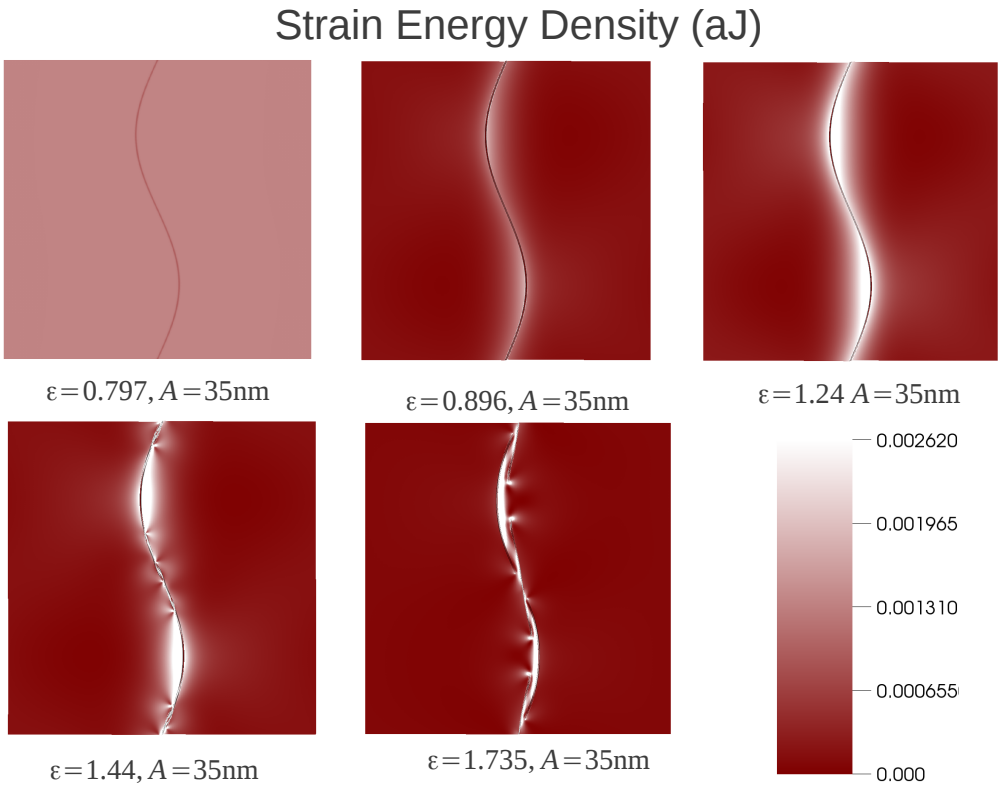

Figure 3.5: Variation of total Strain Energy for different Amplitudes

bending in both the directions. This bending along the sinusoidal path results in a non-zero Gaussian curvature at the folds implying stretching in the Graphene layer. Also when the strain is increased once the fold is formed, we find that the strain energy again begins to rise. This is because as we increase the strain, the size or height of the fold also increases and hence results in an increase in the Gaussian Curvature which causes this rise in strain energy. After a certain increase, the second relaxation is due to breaking of the curved fold to smaller straighter segments. For a higher amplitude we see that this relaxation occurs at an earlier strain itself. For the simulation with A = 0 nm, *i.e.* a straight folding pattern, the strain energy does not increase with strain. This is because, for a straight fold, as there is no bending in the Y-direction, one of the principal curvatures is zero and hence the Gaussian curvature is a constant zero and the strain energy remains more or less constant.

Fig. 3.5 shows the Strain energy density of Graphene for a simulation with an amplitude of 35 nm at different strains. We see that initially until the fold has formed ($\epsilon = 0.797\%$ in 3.5) the strain energy more or less remains constant over the entire region and as we increase the strain, then strain

energy redistributes and it is focussed at the region containing the folds. At a strain of $\epsilon = 1.44\%$ the fold starts to break and the strain energy is now concentrated again at the breaking points.

3.3.2 Bending Energy

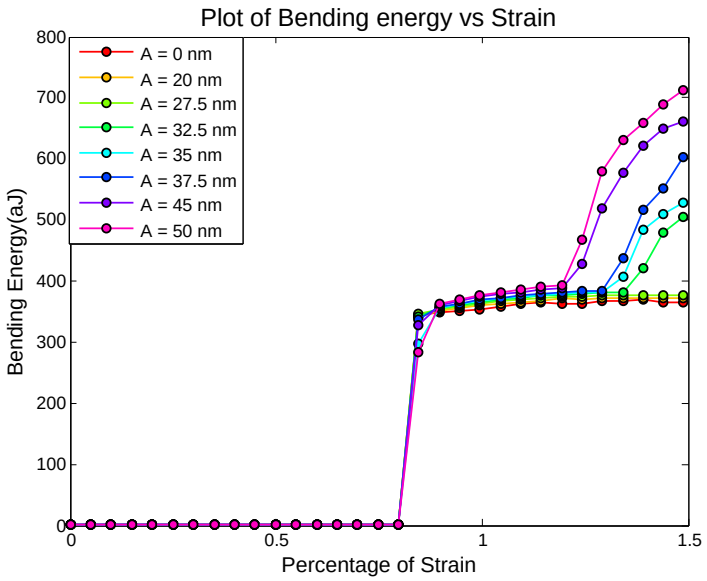

Figure 3.6: Variation of Bending Energy for different Amplitudes

From the pictures of the curved folds in 3.1, we see that there is bending of the graphene both in the X (along fold) and Y (along sine curve) direction. This results in a significant bending energy. Fig. 3.6 shows the bending energy for the simulations for different amplitudes with strain. From the figure we can see that initially until the fold is formed there is no bending energy and then the bending energy suddenly rises. This is due to the formation of fold at a strain of $\epsilon = 0.797\%$. As we keep increasing the strain, we see that the bending energy more or less remains constant. Thus, we can conclude that the fragmentation of folds to smaller segments is due to the effect of the in-plane strain energy and not the bending energy. As we keep increasing the strain, we see that the bending energy again increases. This is due to the breaking of the folds into smaller segments. From 3.3 we see that once the folds are formed, the length of the folds also increases (sum of lengths

of the fragments is greater than the arclength of the sinusoidal fold before fragmentation). Thus this increase in bending energy can be attributed to increase in the length of the fold.

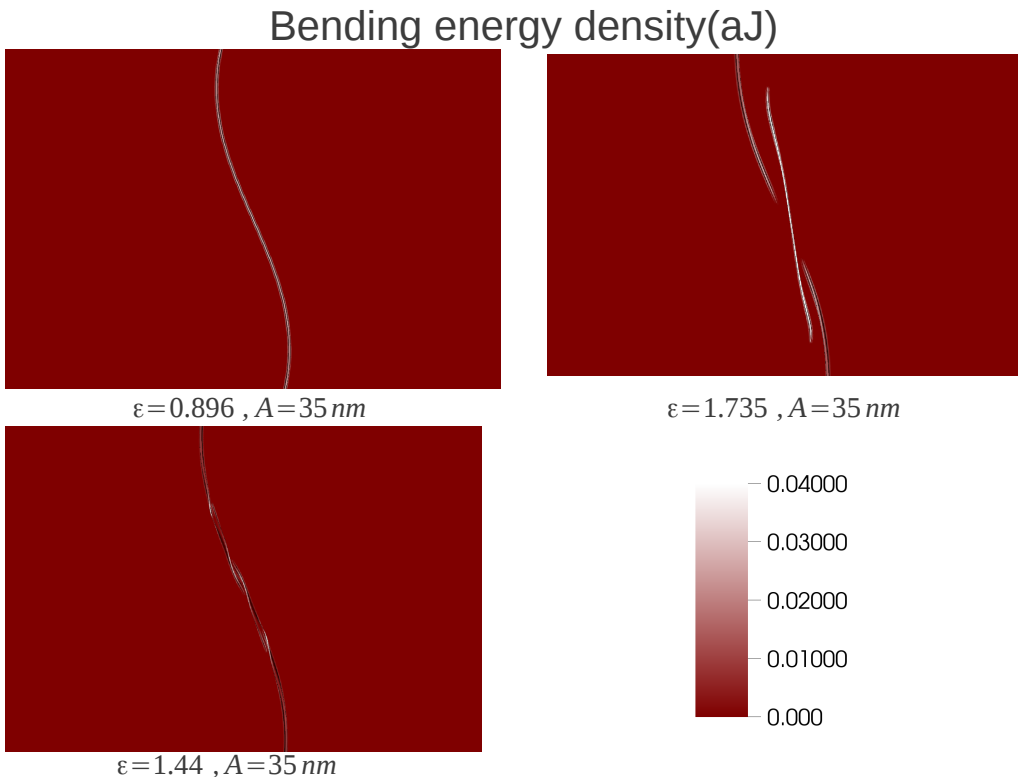

Figure 3.7: Bending energy density of graphene

Fig 3.7 shows the bending energy density profile for the Graphene layer. Initially, when there is no fold, the bending energy is almost zero (as seen in 3.6) but once the folds are formed, the bending energy is concentrated at the fold. As the bending energy depends on the curvature of the fold, we find that in 3.7 the bending energy is maximum at the centre of the fold. As we keep increasing the strain and once the curved fold breaks, the bending energy is maximum at the places where the breaking occurs as there is huge distortion in these places.

3.3.3 Van der Waals Energy

The Van der Waals energy is the interaction energy between the graphene layer and the SiO_2 substrate and is given by the Lennard-Jones Potential (see section 2.2.2). Figure 3.8 shows the relative Van der Waals energy with

respect to the uncompressed state. We can see that till the fold is formed, there is no change in the Van der Waals energy and it suddenly increases due to the formation of the fold. The Van der Waals energy again increases when the fold grows. This is mainly because of two reasons, firstly being the increase in separation between graphene and the substrate and secondly as the fold grows, more and more atoms come into the adhesion free zone causing further increase in the interaction energy (decrease in magnitude). Once the fold breaks into fragments, the Van der Waals energy again increases due to the increase in the length of folds as explained in 3.3.2

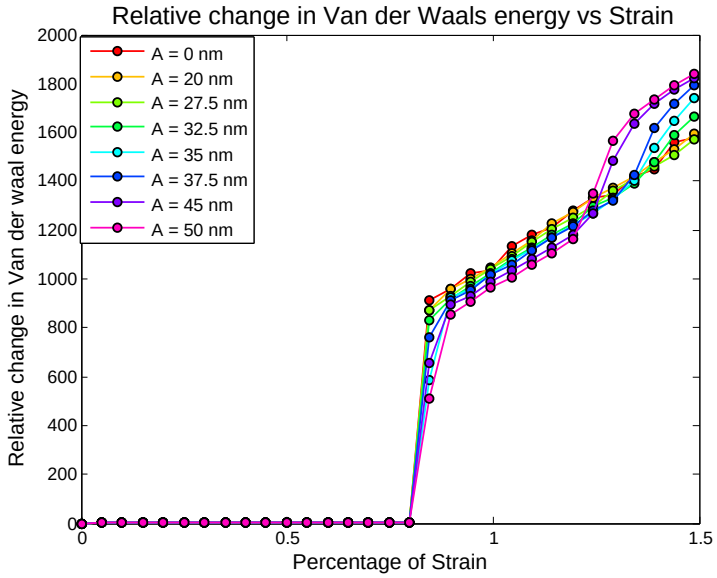

Figure 3.8: Relative change in Van der Waals Energy with strain for different Amplitudes

Fig 3.9 shows the Van der waals Energy density distribution in the Graphene layer. As the Van der Waals energy depends on the separation between the Graphene layer and the substrate, at the places where the fold is formed, the Van der Waals interaction is very less and at the other places, there is significant Van der Waals energy. This can be clearly seen in the Van der Waals energy distribution in 3.9

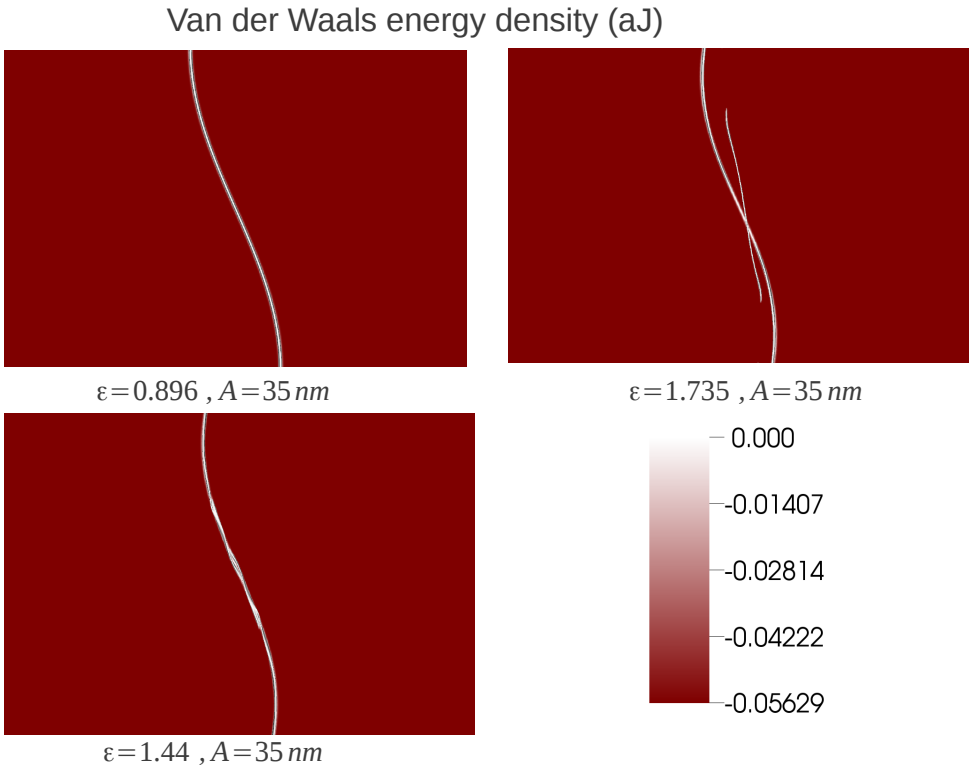

Figure 3.9: Van der Waals energy density along Graphene layer, (*Please note the difference in the scales for each subplot*)

Chapter 4

Conclusion

We have found that it is possible to create curved folds in uniaxially compresssed graphene on a substrate by patterning the substrate into regions of weak adhesion. As the curvature of the fold increases or the compressive strain increases, the curved fold breaks into smaller segments as a relaxation mechanism. The fragmentation strain also depends on the curvature of the folds and for a higher curvature, the fold fragmentation strain is found to be lower. Once the fold is formed, the stretching energy continues to increase under compressive strain while the bending energy more or less remains constant. This suggests that the second relaxation to fragmentation of folds is mainly caused to relax the in-plane strain energy. These curved folds can have interesting applications in focussing graphene plasmonic waves for nanoelectronic devices or in nanofluidics.

Bibliography

P. R. Wallace. The band theory of graphite. *Phys. Rev.*, 71:622–634, May 1947. doi:10.1103/PhysRev.71.622.

J. C. Slonczewski and P. R. Weiss. Band structure of graphite. *Phys. Rev.*, 109:272–279, Jan 1958. doi:10.1103/PhysRev.109.272.

K. S. Novoselov, A. K. Geim, S. V. Morozov, D. Jiang, Y. Zhang, S. V. Dubonos, I. V. Grigorieva, and A. A. Firsov. Electric field effect in atomically thin carbon films. *Science*, 306(5696):666–669, 2004. doi:10.1126/science.1102896.

A. K. Geim and K. S. Novoselov. The rise of graphene. *Nat Mater*, 6: 1476–1122, 2007. doi:10.1038/nmat1849.

Raji Heyrovska. Atomic structures of graphene, benzene and methane with bond lengths as sums of the single, double and resonance bond radii of carbon. *General Physics, arXiv*, 2008. doi:arXiv:0804.4086.

Gordon E. Moore. Cramming more components onto integrated circuits. *Electronics*, 38(8), 1965.

A. H. Castro Neto, F. Guinea, N. M. R. Peres, K. S. Novoselov, and A. K. Geim. The electronic properties of graphene. *Rev. Mod. Phys.*, 81:109–162, Jan 2009. doi:10.1103/RevModPhys.81.109.

A. H. Castro Neto, F. Guinea, and N. M. R. Peres. Drawing conclusions from graphene. *Phy. World.*, 19:33, 2006a.

Novoselov K. S. Katsnelson M. I. and Geim A. K. Chiral tunnelling and the klein paradox in graphene. *Nat Phy*, 2(1745-2473):620–625, 2006. doi:10.1038/nphys384.

M.I. Katsnelson and K.S. Novoselov. Graphene: New bridge between condensed matter physics and quantum electrodynamics. *Solid*

State Communications, 143(1–2):3 – 13, 2007. ISSN 0038-1098. doi:10.1016/j.ssc.2007.02.043. ¡ce:title¿Exploring graphene¡/ce:title¿ ¡ce:subtitle¿Recent research advances¡/ce:subtitle¿.

A. H. Castro Neto, F. Guinea, and N. M. R. Peres. Edge and surface states in the quantum hall effect in graphene. *Phys. Rev. B*, 73:205408, May 2006. doi:10.1103/PhysRevB.73.205408.

Morozov S. V. et al Novoselov K. S., Geim A. K. Two-dimensional gas of massless dirac fermions in graphene. *Nature*, 438:197–200, 2005. doi:10.1038/nature04233.

Changgu Lee, Xiaoding Wei, Jeffrey W. Kysar, and James Hone. Measurement of the elastic properties and intrinsic strength of monolayer graphene. *Science*, 321(5887):385–388, 2008. doi:10.1126/science.1157996.

Alexander A. Balandin, Suchismita Ghosh, Wenzhong Bao, Irene Calizo, Desalegne Teweldebrhan, Feng Miao, and Chun Ning Lau. Superior thermal conductivity of single-layer graphene. *Nano Letters*, 8(3):902–907, 2008. doi:10.1021/nl0731872. PMID: 18284217.

Masa Ishigami, J. H. Chen, W. G. Cullen, M. S. Fuhrer, and E. D. Williams. Atomic structure of graphene on sio2. *Nano Letters*, 7(6):1643–1648, 2007. doi:10.1021/nl070613a.

J. Sabio, C. Seoánez, S. Fratini, F. Guinea, A. H. Castro Neto, and F. Sols. Electrostatic interactions between graphene layers and their environment. *Phys. Rev. B*, 77:195409, May 2008. doi:10.1103/PhysRevB.77.195409.

Nicolas Camara Benoit Jouault Bilal Jabakhanji Alessandra Caboni Antoine Tiberj Christophe Consejo Philipe Godignon and Jean Camassel. Multidimensional characterization, landau levels and density of states in epitaxial graphene grown on sic substrates. *Nanoscale Research Letters*, 6(141), 2011. doi:10.1186/1556-276X-6-141.

Claire Berger, Zhimin Song, Tianbo Li, Xuebin Li, Asmerom Y. Ogbazghi, Rui Feng, Zhenting Dai, Alexei N. Marchenkov, Edward H. Conrad, Phillip N. First, and Walt A. de Heer. Ultrathin epitaxial graphite 2d electron gas properties and a route toward graphene-based nanoelectronics. *The Journal of Physical Chemistry B*, 108(52):19912–19916, 2004. doi:10.1021/jp040650f.

Claire Berger, Zhimin Song, Xuebin Li, Xiaosong Wu, Nate Brown, Cécile Naud, Didier Mayou, Tianbo Li, Joanna Hass, Alexei N. Marchenkov,

Edward H. Conrad, Phillip N. First, and Walt A. de Heer. Electronic confinement and coherence in patterned epitaxial graphene. *Science*, 312 (5777):1191–1196, 2006. doi:10.1126/science.1125925.

Yi Zhang, Luyao Zhang, and Chongwu Zhou. Review of chemical vapor deposition of graphene and related applications. *Accounts of Chemical Research*, 2013. doi:10.1021/ar300203n.

Xuesong Li, Weiwei Cai, Jinho An, Seyoung Kim, Junghyo Nah, Dongxing Yang, Richard Piner, Aruna Velamakanni, Inhwa Jung, Emanuel Tutuc, Sanjay K. Banerjee, Luigi Colombo, and Rodney S. Ruoff. Large-area synthesis of high-quality and uniform graphene films on copper foils. *Science*, 324(5932):1312–1314, 2009. doi:10.1126/science.1171245.

K. S. Kim, Y. Zhao, H. Jang, S. Y. Lee, J. M. Kim, K. S. Kim, J. H. Ahn, P. Kim, J.Y. Choi, and B. H. Hong. Large-scale pattern growth of graphene films for stretchable transparent electrodes. *Nature*, 457(7230): 706–710, 2009. doi:10.1038/nature07719.

Cecilia Mattevi, Hokwon Kim, and Manish Chhowalla. A review of chemical vapour deposition of graphene on copper. *J. Mater. Chem.*, 21:3324–3334, 2011. doi:10.1039/C0JM02126A.

Teng Li and Zhao Zhang. Substrate-regulated morphology of graphene. *Journal of Physics D: Applied Physics*, 43(7):075303, 2010.

Scott Scharfenberg, Nikhita Mansukhani, Cesar Chialvo, Richard L. Weaver, and Nadya Mason. Observation of a snap-through instability in graphene. *Applied Physics Letters*, 100(2):021910, 2012. doi:10.1063/1.3676059.

J. C. Meyer, Geim A. K., Katsnelson M. I., Novoselov K. S., Booth T. J., and Roth S. The structure of suspended graphene sheets. *Nature*, 446 (7131):60–63, 2007. doi:10.1038/nature05545.

Anchal Srivastava, Charudatta Galande, Lijie Ci, Li Song, Chaitra Rai, Deep Jariwala, Kevin F. Kelly, and Pulickel M. Ajayan. Novel liquid precursor-based facile synthesis of large-area continuous, single, and few-layer graphene films. *Chemistry of Materials*, 22(11):3457–3461, 2010. doi:10.1021/cm101027c.

Bao Wenzhong Miao Feng Chen Zhen Zhang Hang Jang Wanyoung Dames Chris and Lau Chun Ning. Controlled ripple texturing of suspended graphene and ultrathin graphite membranes. *Nat Nano*, 4(1748-3387): 562–566, 2009. doi:10.1038/nnano.2009.191.

J B Nelson and D P Riley. The thermal expansion of graphite from 15 to 800 degrees Celsius: part I. Experimental. *Proceedings of the Physical Society*, 57(6):477, 1945.

A. L. Vázquez de Parga, F. Calleja, B. Borca, M. C. G. Passeggi, J. J. Hinarejos, F. Guinea, and R. Miranda. Periodically rippled graphene: Growth and spatially resolved electronic structure. *Phys. Rev. Lett.*, 100: 056807, Feb 2008. doi:10.1103/PhysRevLett.100.056807.

Eun-Ah Kim and A. H. Castro Neto. Graphene as an electronic membrane. *EPL (Europhysics Letters)*, 84(5):57007, 2008.

F. Guinea, M. I. Katsnelson, and M. A. H. Vozmediano. Midgap states and charge inhomogeneities in corrugated graphene. *Phys. Rev. B*, 77:075422, Feb 2008a. doi:10.1103/PhysRevB.77.075422.

F. Guinea, Baruch Horovitz, and P. Le Doussal. Gauge field induced by ripples in graphene. *Phys. Rev. B*, 77:205421, May 2008b. doi:10.1103/PhysRevB.77.205421.

M.I Katsnelson and A.K Geim. Electron scattering on microscopic corrugations in graphene. *Philosophical Transactions of the Royal Society A: Mathematical, Physical and Engineering Sciences*, 366(1863):195–204, 2008. doi:10.1098/rsta.2007.2157.

D. C. Elias, R. R. Nair, T. M. G. Mohiuddin, S. V. Morozov, P. Blake, M. P. Halsall, A. C. Ferrari, D. W. Boukhvalov, M. I. Katsnelson, A. K. Geim, and K. S. Novoselov. Control of graphene's properties by reversible hydrogenation: Evidence for graphane. *Science*, 323(5914):610–613, 2009. doi:10.1126/science.1167130.

Vitor M. Pereira and A. H. Castro Neto. Strain engineering of graphene's electronic structure. *Phys. Rev. Lett.*, 103:046801, Jul 2009.

Hugues Vandeparre, Julien Léopoldès, Christophe Poulard, Sylvain Desprez, Gwennaelle Derue, Cyprien Gay, and Pascal Damman. Slippery or sticky boundary conditions: Control of wrinkling in metal-capped thin polymer films by selective adhesion to substrates. *Phys. Rev. Lett.*, 99:188302, Oct 2007. doi:10.1103/PhysRevLett.99.188302.

Hayward RC Chan EP, Smith EJ and Crosby AJ. Surface wrinkles for smart adhesion. *Advanced Materials*, 20(4):711–716, 2008. ISSN 1521-4095. doi:10.1002/adma.200701530.

K. Zhang and M. Arroyo. Adhesion and friction control localized folding in supported graphene. *Journal of Applied Physics*, 113(19):193501, 2013. doi:10.1063/1.4804265.

Marino Arroyo and Ted Belytschko. An atomistic-based finite deformation membrane for single layer crystalline films. *Journal of the Mechanics and Physics of Solids*, 50(9):1941 – 1977, 2002. ISSN 0022-5096. doi:http://dx.doi.org/10.1016/S0022-5096(02)00002-9.

M. Arroyo and T. Belytschko. Finite element methods for the non-linear mechanics of crystalline sheets and nanotubes. *International Journal for Numerical Methods in Engineering*, 59(3):419–456, 2004. ISSN 1097-0207. doi:10.1002/nme.944.

Fehmi Cirak, Michael Ortiz, and Peter Schröder. Subdivision surfaces: a new paradigm for thin-shell finite-element analysis. *International Journal for Numerical Methods in Engineering*, 47(12):2039–2072, 2000. ISSN 1097-0207. doi:10.1002/(SICI)1097-0207(20000430)47:12<2039::AID-NME872>3.0.CO;2-1.

F. Morgan. *Riemannian Geometry, a beginner's guide*. Jones and Barlett Publishers, Boston, MA, 1993.

Donald W. Brenner. Empirical potential for hydrocarbons for use in simulating the chemical vapor deposition of diamond films. *Phys. Rev. B*, 42: 9458–9471, Nov 1990. doi:10.1103/PhysRevB.42.9458.

L. A. Girifalco, Miroslav Hodak, and Roland S. Lee. Carbon nanotubes, buckyballs, ropes, and a universal graphitic potential. *Phys. Rev. B*, 62: 13104–13110, Nov 2000. doi:10.1103/PhysRevB.62.13104.

Zachary H. Aitken and Rui Huang. Effects of mismatch strain and substrate surface corrugation on morphology of supported monolayer graphene. *Journal of Applied Physics*, 107(12):123531, 2010. doi:10.1063/1.3437642.

Marcelo A. Dias and Christian D. Santangelo. The shape and mechanics of curved-fold origami structures. *EPL (Europhysics Letters)*, 100(5):54005, 2012. doi:10.1209/0295-5075/100/54005.